QUALITY CONTROL PROCEDURES FOR SOLAR RADIATION DATA IN NORTHERN CHILE

Luis A. Conde[1,2]*, Douglas Olivares[1,2], Abel Taquichiri[2], Josefa Montoya[2], Edward Fuentealba[1,2], Aitor Marzo[3,4]

[1]Solar Energy Research Center, Universidad de Chile, Tupper 2007, Santiago, 8370451, Chile

[2]Centro de Desarrollo Energético Antofagasta, Universidad de Antofagasta, Angamos 601, Antofagasta, 1270300, Chile

[3]Department of Optics, University of Granada, Profesor Adolfo Rancaño St., 18071, Granada, Spain

[4]CIESOL, Joint Centre of the University of Almería-CIEMAT, 04120, Almería, Spain

*Corresponding author: luis.conde.mendoza@ua.cl

Abstract

Data quality control is essential to ensure the reliability of research and analysis results. Terrestrial measurements of solar radiation often present intermittency, randomness, and uncertainty, which may lead to errors. Quality control procedures help detect erroneous, missing, or anomalous data caused by factors such as instrument cleaning, miscalibration, sensor imbalance, or communication issues. This study evaluates validation methods for ground-based irradiance measurements in the Atacama Desert and the city of Antofagasta, northern Chile. The three components of global irradiance were analyzed independently and in combination, complemented by color-based visualization of distribution patterns over time. This approach allowed the identification of valid, anomalous, and missing data. Most anomalies were linked to tracking system failures, with unevenness and soiling as minor contributors. The results demonstrated that the proposed methodology effectively filtered and detected common errors, while visual analysis supported the inspection and diagnosis of anomalies in the measurements.

Keywords: Data quality control, Solar irradiance validation, Time series, Anomaly detection, Visual analysis

1. Introduction

Northern Chile, particularly the Antofagasta region and the Atacama Desert, is among the most irradiated areas in the world, making it an ideal location for solar energy generation (Olivares et al. 2025). The Atacama Desert, characterized by arid and cloudless conditions, records horizontal global radiation values exceeding 8 kWh/m² per day (Marzo et al. 2017), offering exceptional potential for photovoltaic (PV) energy production. Additionally, the installation of PV plants in these desert regions minimizes land use conflicts by avoiding arable or habitable areas. The city of Antofagasta, located on the Pacific coast near the desert, also experiences high irradiance levels, but with local atmospheric variability and greater cloudiness that can affect data stability and measurement accuracy.

Ensuring the accuracy and quality of solar irradiance data is essential for the optimal design, sizing, and operation of PV systems. However, extreme environmental conditions, sensor degradation, and microclimatic contrasts between desert and coastal environments pose challenges for consistent data collection. Measurement errors may lead to under- or overestimation of energy potential, impacting both system performance and financial feasibility. Although several studies have highlighted the solar potential of northern Chile, most have focused on energy generation rather than the quality and consistency of solar irradiance data. Previous research in Morocco (El Alani et al. 2021), Argentina (Nollas, Salazar, and Gueymard 2023), and other regions (Forstinger et al. 2021) has proposed various quality control methodologies to identify and filter erroneous measurements using multi-year ground-based datasets. These studies emphasize the need for improved automated quality control approaches to ensure data integrity while reducing expert validation costs.

This study aims to analyze and compare the quality of solar irradiance data collected at two representative sites in northern Chile—the Atacama Desert and the city of Antofagasta. The objective is to identify measurement errors, assess data reliability, and adapt existing quality control methodologies to the region's unique environmental conditions. One-minute measurements of the three components of solar irradiance were analyzed to detect anomalies and enhance the accuracy and consistency of irradiance datasets used for solar energy research and applications.

10.18086/swc.2025.04.37 Available at http://proceedings.ises.org

2. Study sites and data status

2.1. Measurement sites and instrumentation

Irradiance data for this study were collected from two ground-based stations located in northern Chile: *Solar Platform of Atacama Desert* (PSDA) and the *Centro de Desarrollo Energético Antofagasta* (CDEA). The PSDA station is situated at 24.09° S, 69.93° W and 965 m a.s.l. in the Atacama Desert, an area characterized by extreme aridity and classified as a hot desert climate (BW) according to the Köppen–Geiger classification (Kottek et al. 2006). It has been in continuous operation since 2017 (Marzo et al. 2017). The CDEA station, located at 23.71° S, 70.42° W and 23 m a.s.l. within the University of Antofagasta campus, operates under a coastal desert climate (BWk) and began measurements in 2022. The two sites are approximately 65 km apart, providing complementary data from inland and coastal desert environments (Figure 1 and Figure 2).

Figure 1: PSDA ground-based station, located in the Atacama Desert (24.09°S, 69.93°W) at 965 m a.s.l., with systems and radiometric instruments operating under extreme arid conditions.

Figure 2: CDEA ground-based station, located in the University of Antofagasta (23.71°S, 70.42°W) at 23 m a.s.l., with systems and radiometric instruments operating in a coastal desert environment.

Both stations acquire irradiance data at a 1-minute temporal resolution and follow international standards for radiometric monitoring (ISO 9060:2018; ISO 9847:1992). Global Horizontal Irradiance (GHI) is measured using Kipp & Zonen CMP22 and CMP11 pyranometers, classified as secondary standard and ISO 9060 Class A, respectively, and mounted on horizontal, shadow-free platforms. Diffuse Horizontal Irradiance (DHI) is measured with the same type of pyranometers mounted on SOLYS-2 dual-axis solar trackers equipped with shading devices. Direct Normal Irradiance (DNI) is measured with Kipp & Zonen CHP1 pyrheliometers mounted on the same SOLYS-2 trackers, with a tracking accuracy of ±0.1°. At PSDA, an upward-facing Kipp & Zonen CMA11 albedometer (dual hemisphere, 285–2800 nm) was also installed to measure surface albedo.

2.2. Preliminary visual inspection

A preliminary analysis using heat maps of irradiance versus time was conducted to identify trends, data gaps, and anomalies in the one-minute GHI, DNI, and DHI records (El Alani et al. 2021)(repositorio.smn.gob.ar et al. 2024). At PSDA (Figure 3), about eight months of missing data were detected, mainly in 2022. The GHI plot (Figure 3a) showed consistent patterns, with few extreme values exceeding 1200 W/m². In contrast, the DNI (Figure 3b) and DHI (Figure 3c) plots displayed anomalies in 2021, likely caused by solar tracker misalignment, characterized by low DNI (<10 W/m²) and overestimated DHI (>250 W/m²) values.

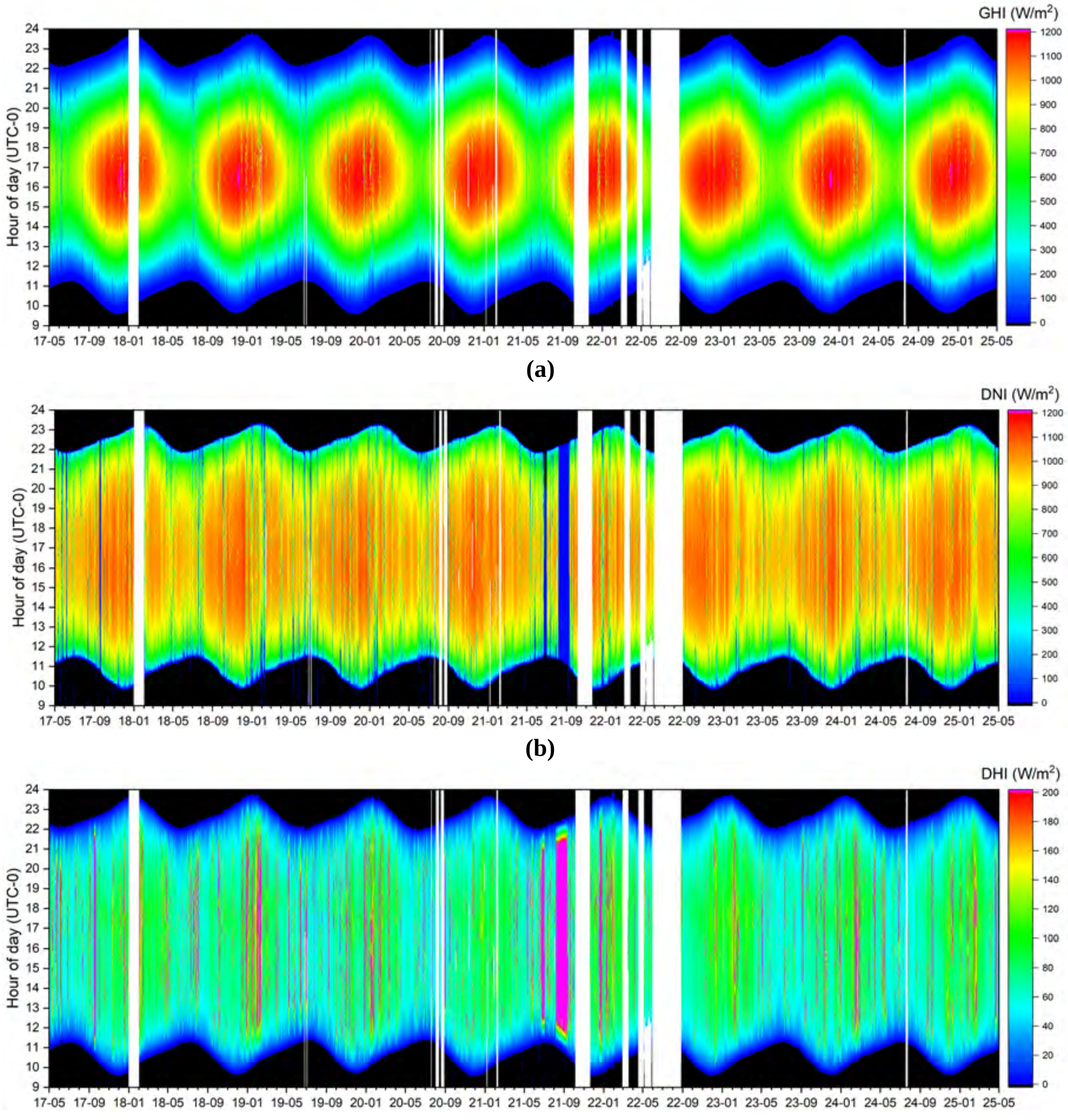

Figure 3: Heat maps for PSDA station: (a) GHI, (b) DNI, and (c) DHI, showing missing data and anomalies.

At CDEA (Figure 4), data loss was limited to roughly two weeks in 2022. The GHI pattern (Figure 4a) remained stable, while DHI and DNI (Figures 4b and 4c) exhibited inconsistencies during 2023, including a three-month period of misalignment and a delayed start of approximately two hours after sunrise from mid-2023 onward, likely due to tracking or calibration issues.

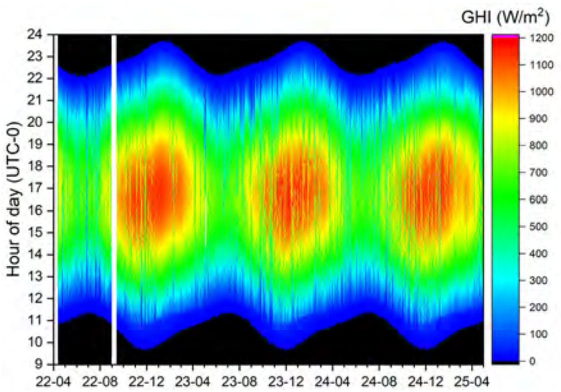

(a)

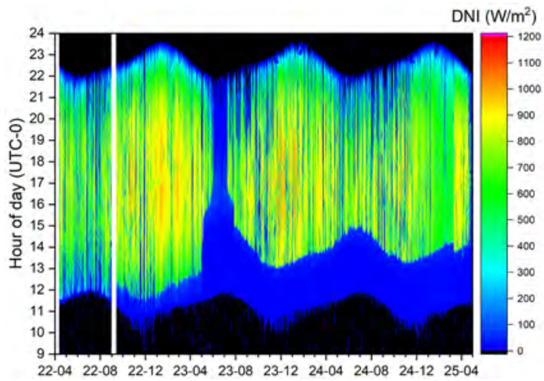

(b)

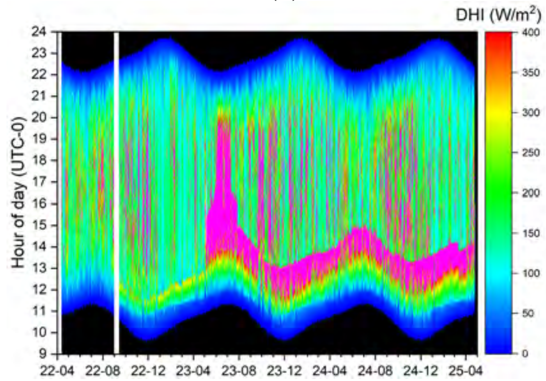

(c)

Figure 4: Heat maps for CDEA station: (a) GHI, (b) DNI, and (c) DHI, showing missing data and anomalies.

3. Quality control methods

3.1. One-component analysis

To identify erroneous data, the tests Physically Possible Limits (**PPL**) and Extremely Rare Limits (**ERL**) were considered according to BSRN quality control (Long and Shi 2006)(El Alani et al. 2021).

- **BSRN-PPL:**

$$GHI < 1.50 \times ETN\ (\cos(SZA))^{1.2} + 100\, W/m^2, \text{ for } SZA < 90° \qquad \text{(eq. 1)}$$

$$DHI < 0.95 \times ETN\ (\cos(SZA))^{1.2} + 50\, W/m^2, \text{ for } SZA < 90° \qquad \text{(eq. 2)}$$

- **BSRN-ERL:**

$$GHI < 1.20 \times ETN\ (\cos(SZA))^{1.2} + 50\, W/m^2, \text{ for } SZA < 90° \qquad \text{(eq. 3)}$$

$$DHI < 0.75 \times ETN\ (\cos(SZA))^{1.2} + 30\, W/m^2, \text{ for } SZA < 90° \qquad \text{(eq. 4)}$$

where ETN is the extraterrestrial irradiance at normal incidence (1367 W/m^2), and SZA is the solar zenith angle. The SZA and elevation were calculated by the PVLIB toolbox for Python (Anderson et al. 2023).

Figure 5(a) and Figure 5(b) show the one-component analysis for the GHI in PSDA and CDEA, respectively. In PSDA and CDEA there were points above the ERL level or the solar constant, at low zenith angles, which could be due to overirradiance events (Zamalloa-Jara et al. 2023).

Figure 6(a) and Figure 6(b) show the one-component analysis for the DHI. Points were found between the PPL and ERL levels, which are mainly due to sensor misalignment problems (Zo et al. 2017).

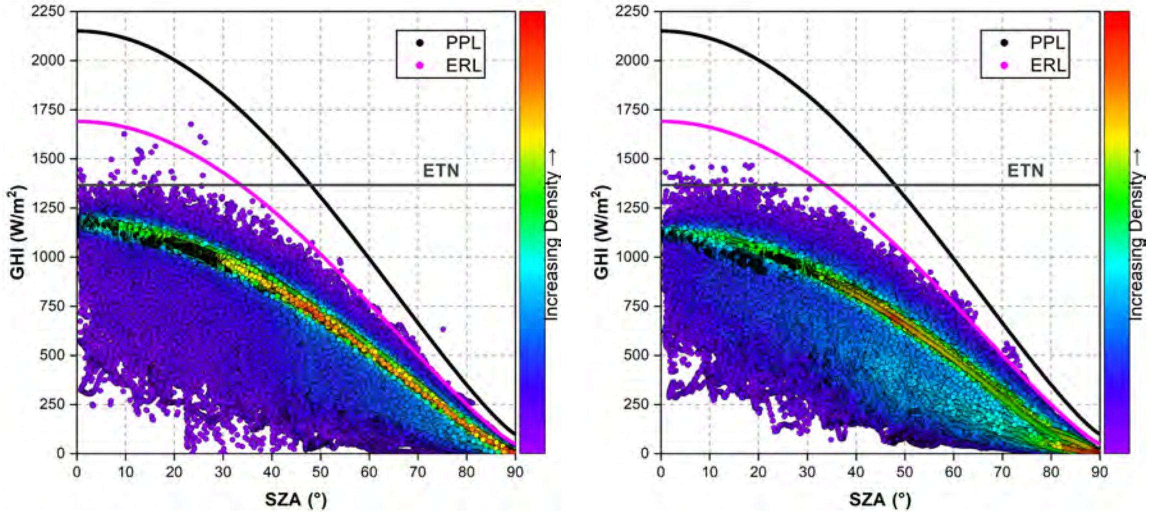

(a) (b)

Figure 5: GHI vs SZA in (a) PSDA and (b) CDEA with PPL and ERL limits from BSRN.

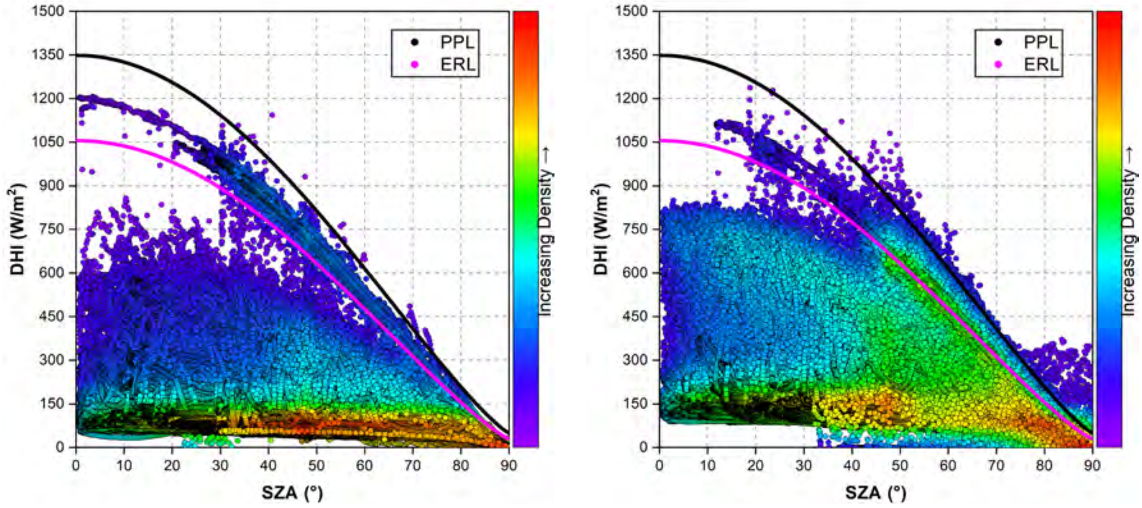

(a) (b)

Figure 6: DHI vs SZA in (a) PSDA and (b) CDEA with PPL and ERL limits from BSRN.

3.2. Two-component analysis

This analysis is often used in the dimensionless "**K**" space, proposed by NREL (Maxwell et al., 1993). This is a well-known methodology used in the literature, the quality of the irradiance data is evaluated based on the direct and diffuse transmittances and the clearness index (Zo et al. 2017)(El Alani et al. 2021).

Clearness index ($\boldsymbol{K_t}$) or the global horizontal transmittance:

$$K_t = \frac{GHI}{ETN\cos(SZA)} \tag{eq. 5}$$

Diffuse transmittance ($\boldsymbol{K_d}$)

$$K_d = \frac{DHI}{GHI} \tag{eq. 6}$$

Direct beam transmittance ($\boldsymbol{K_n}$)

$$K_n = \frac{DNI}{ETN} \tag{eq. 7}$$

Figure 7 and Figure 8 show the $K_d - K_t$ and $K_n - K_t$ density plots, respectively, for PSDA and CDEA stations.

For this analysis, cases meeting the following conditions were considered: $50 < GTI, SZA < 90°$, $0 < DHI < 1500$, $0 < DNI$, and $0 < K_d < 1$. These constraints remove low-irradiance and high-SZA conditions that increase pyranometer uncertainty (Nollas, Salazar, and Gueymard 2023) and exclude physically implausible data caused by shading or connection errors. Figure 7(a) and Figure 7(b) illustrate the $K_d - K_t$ relationship for the PSDA and CDEA stations, respectively. According to (Gueymard and Ruiz-Arias 2016):

- $0.9 < K_d < 1 \rightarrow$ overcast ($K_t < 0.6$) and overcast with high albedo ($K_t > 0.6$)
- $0.25 < K_d < 0.9 \rightarrow$ partly cloudy ($K_t < 0.8$) or enhanced by cloud/albedo effects ($K_t > 0.8$)
- $0 < K_d < 0.25 \rightarrow$ clear sky conditions

At PSDA (Figure 7a), the high concentration of points at low K_d and high K_t indicates predominantly clear-sky conditions, with few cloudy or high-albedo cases typical of desert environments. In contrast, CDEA (Figure 7b) shows a broader distribution with moderate K_d values, reflecting more frequent partially cloudy or coastal haze conditions, while still dominated by clear-sky events.

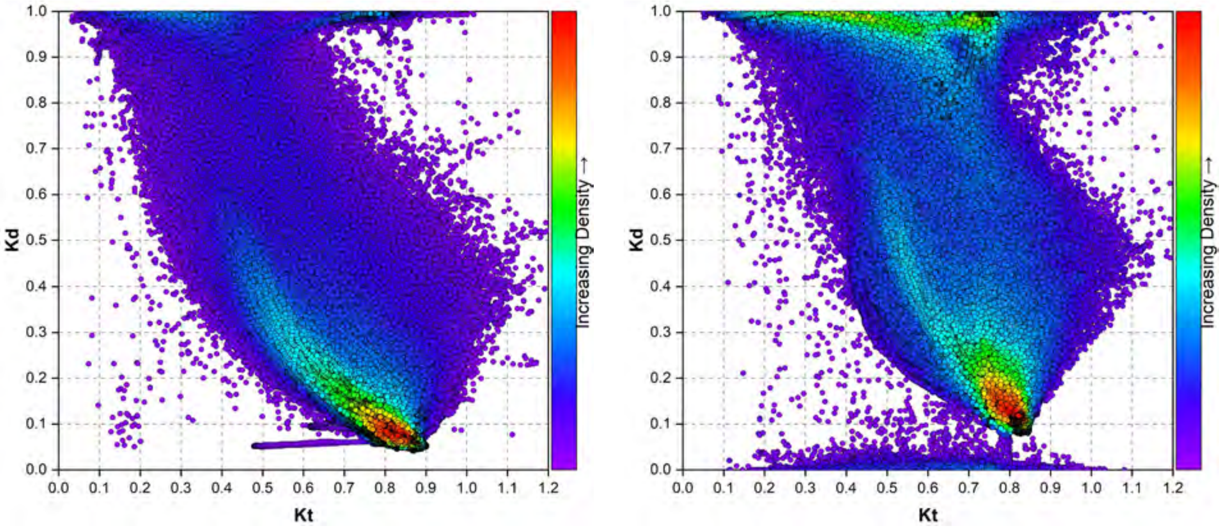

(a) **(b)**

Figure 7: $K_d - K_t$ relationships for PSDA (a) and CDEA (b) stations.

Figure 8(a) and Figure 8(b) show the $K_n - K_t$ density plots for the PSDA and CDEA stations, respectively. These plots illustrate atmospheric attenuation of direct solar irradiance, where K_n values close to 1 indicate clear-sky conditions and minimal atmospheric scattering, while lower values denote increased attenuation (El Alani et al. 2021). Thresholds of 0.8 for PSDA and 0.7 for CDEA were established, reflecting differences in air mass and local atmospheric conditions such as cloud cover, aerosols, and pollution (Younes, Claywell, and Muneer 2005a).

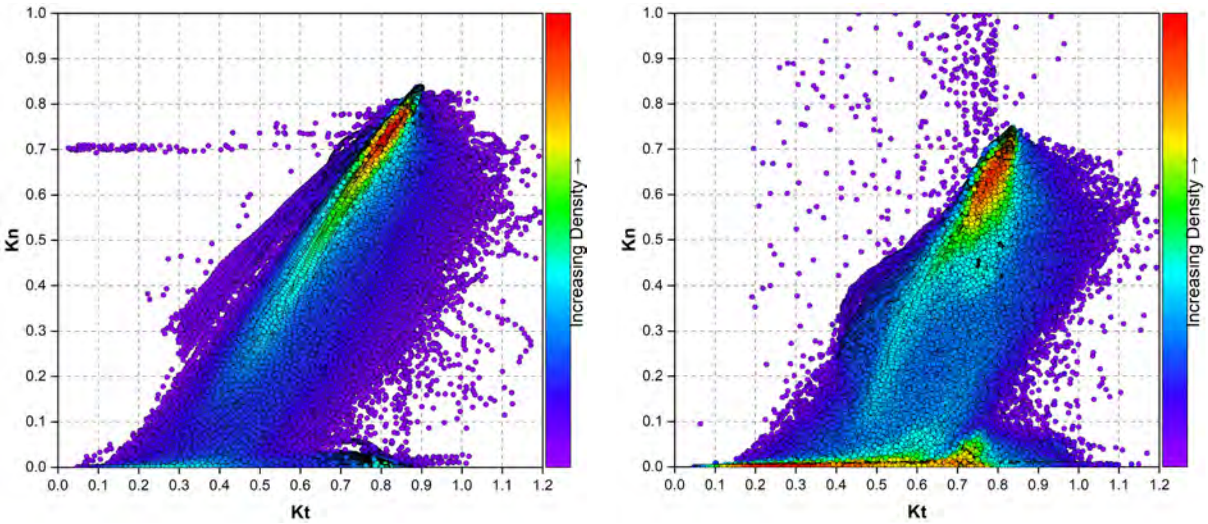

(a) **(b)**

Figure 8: $K_n - K_t$ relationships for PSDA (a) and CDEA (b) stations.

3.3. Three-component analysis

This analysis relates the three irradiance components and is applicable only when GHI, DHI, and DNI are measured simultaneously. The calculated global irradiance (GHI_{cal}) is obtained according to:

$$GHI_{cal} = DHI + DNI \times \cos(SZA) \qquad \text{(eq. 8)}$$

Figures 9a and 9b show the correlation between GHI_{cal} and the measured GHI for the PSDA and CDEA stations, respectively. Data points significantly above the best-fit line suggest potential issues with the GHI sensor, such as shading, soiling, or misalignment, whereas points below the fit line indicate possible alignment errors in the DHI or DNI measurements. To ensure data reliability, only cases with relative errors below 15% between GHI_{cal} and measured GHI were retained for further analysis.

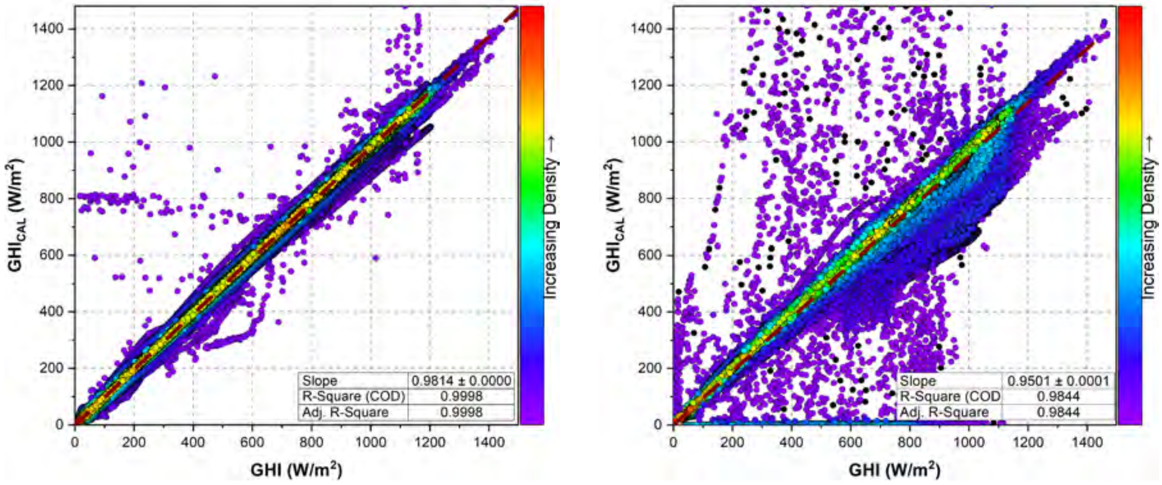

(a) (b)

Figure 9: Correlation between GHI_{cal} vs. GHI for (a) PSDA and (b) CDEA.

4. Results and discussion

4.1. Data Imputation

Figure 10 presents the irradiance data at PSDA after filtering and imputation. As suggested by (Palmer et al. 2018), missing data were reconstructed using measurements from nearby instruments recording the same variable. Prior to imputation, a linear regression validation was performed between datasets to verify consistency and detect potential anomalies. The filtering procedures also helped eliminate anomalous measurements, mainly those caused by tracker misalignment.

In PSDA, approximately five months of missing GHI data in 2021–2022 were recovered using the upward-facing CMP11 sensor from a nearby CMA11 albedometer (Figure 10a). Additional data gaps of a few weeks in 2020 were also filled. For DNI (Figure 10b), about two months of missing data in 2021 were completed using a neighboring pyrheliometer, and non-physical nighttime values were removed. DHI values were reconstructed using Equation (8), primarily for 2021, based on the corrected DNI data (Figure 10c).

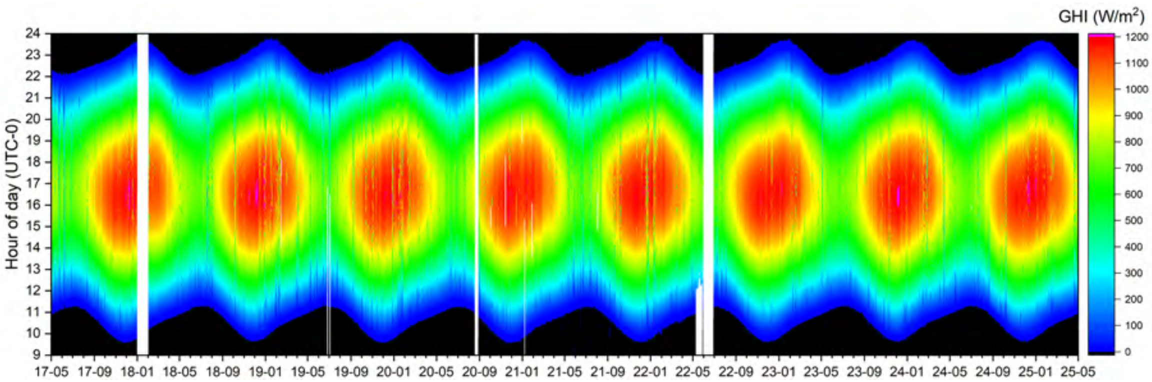

(a)

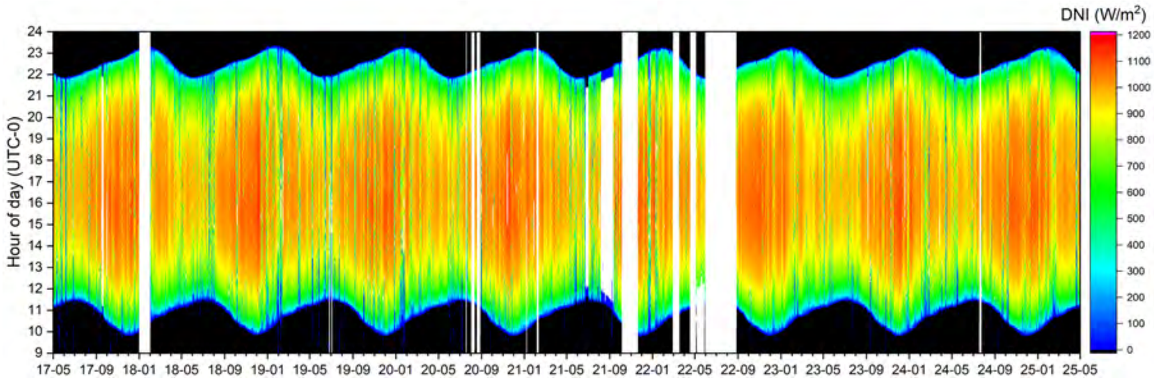

(b)

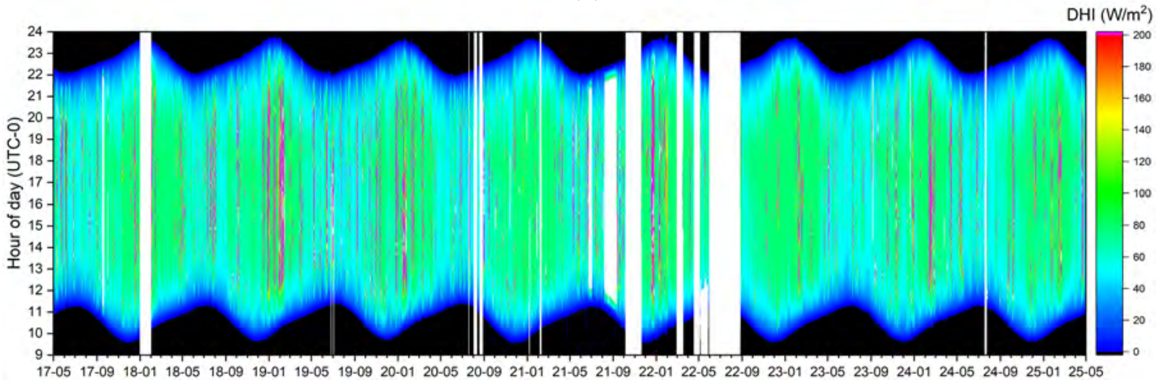

(c)

Figure 10: Heat maps of irradiance at PSDA after data filtering and imputation: (a) GHI with gaps recovered data, (b) DNI completed with auxiliary records, and (c) DHI reconstructed.

For CDEA, Figures 11a and 11b show the filtered DNI and DHI time series. In this case, no redundant instruments were available for cross-imputation; thus, the correction focused on removing anomalous data related to tracker malfunctions, mainly during early morning periods.

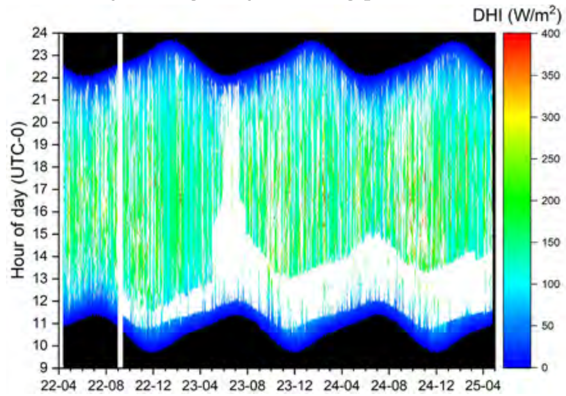

(a)

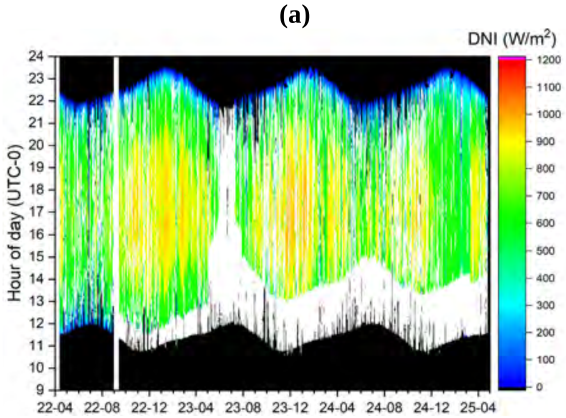

(b)

Figure 11: Time series of filtered irradiance data at CDEA: (a) DHI and (b) DNI after removing anomalous measurements caused by tracker misalignment, mainly during early morning hours.

4.2. Considerations for data filtering

This section presents the one- and two-component analyses performed after visual inspection. Figure 12 shows the one-component analysis for DHI, where a Personalized Experimental Range (PER) was introduced to filter data affected by tracker misalignment. Maximum thresholds of 650 W/m² and 500 W/m² were applied for PSDA and CDEA, respectively. The PER limits were defined as:

$$0.46 \times ETN \times \cos^{1.04}(SZA) + 30\,W/m^2 \qquad \text{(eq. 9)}$$

$$0.35 \times ETN \times \cos^{1.2}(SZA) + 10\,W/m^2 \qquad \text{(eq. 10)}$$

These filters effectively removed anomalous DHI measurements caused by tracker misalignment or temporary sensor obstruction. Since both DHI and DNI are measured on the same SOLYS-2 tracker, the timestamps identified as misaligned in the DHI series were also used to filter corresponding DNI data, ensuring consistent exclusion of tracking-related errors across both components.

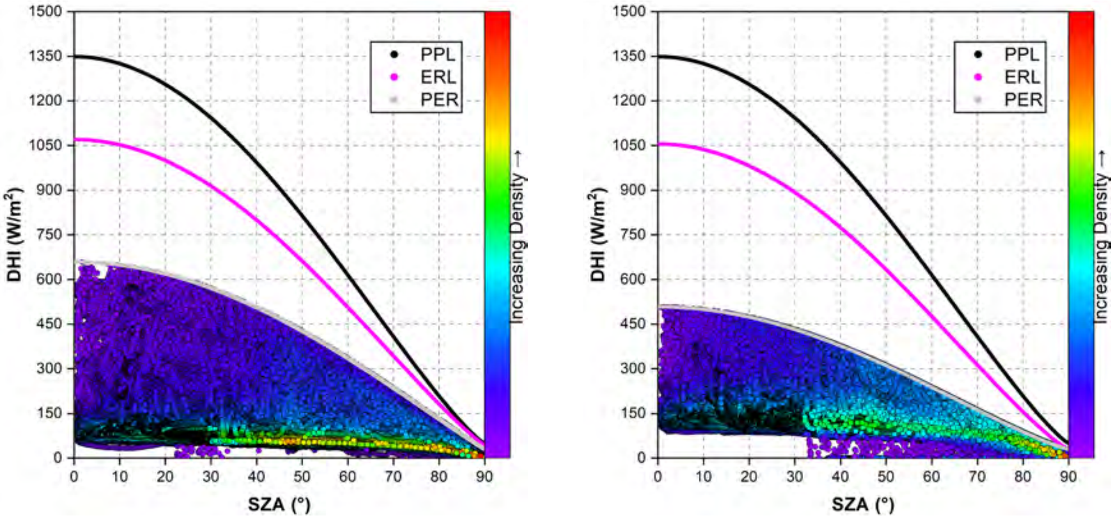

(a) **(b)**

Figure 12: DHI filtered data using one-component analysis for (a) PSDA and (b) CDEA.

Figure 13 shows the resulting K-space diagrams after applying the PER filter. For PSDA (Figure 13a), most points corresponding to cloudy conditions with high albedo (K_d> 0.9 and K_t > 0.6) and partly cloudy conditions with enhanced reflection (K_t > 0.9) were removed. In CDEA (Figure 13b), the PER filtering effectively eliminated points affected by tracker misalignment detected in the one-component analysis, mainly those with unrealistic diffuse fractions. This correction significantly reduced the scatter of data in the $K_d - K_t$ space, resulting in cleaner, denser, and more physically consistent distributions.

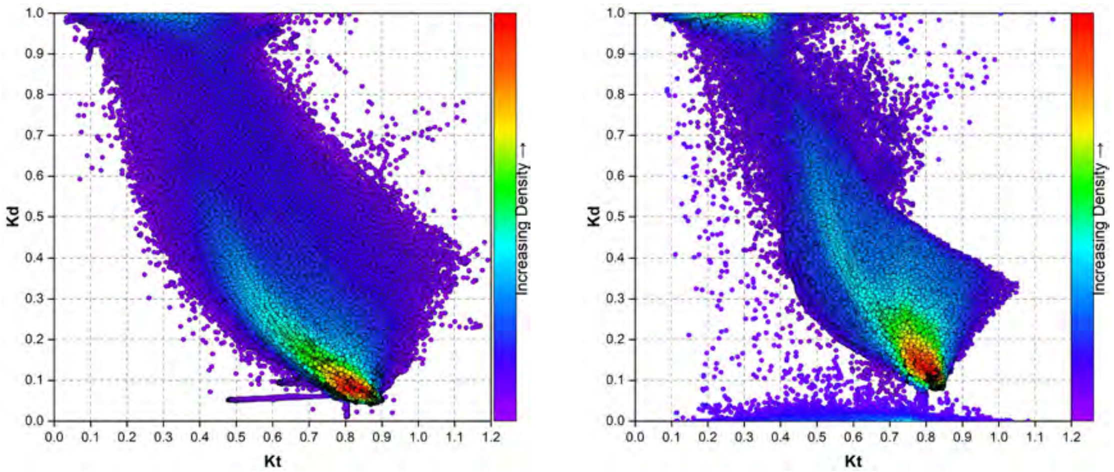

(a) **(b)**

Figure 13: $K_d - K_t$ diagrams for (a) PSDA and (b) CDEA stations, after applying the PER filter; the misalignment-related outliers were removed.

Figure 14 presents the $K_n - K_t$ diagrams for PSDA (a) and CDEA (b) after applying the PER filter. For PSDA, the data exhibit a strong linear correlation, with most points concentrated near $K_n \approx 0.8$, indicating predominantly clear-sky conditions and minimal atmospheric scattering, consistent with the high transparency and low aerosol content of the Atacama Desert atmosphere. Only a few outliers with lower K_n values remain, corresponding to transient cloud passages or temporary tracker misalignment (El Alani et al. 2021). In contrast, CDEA shows a wider dispersion of points and a lower upper limit ($K_n \approx 0.7$), reflecting stronger atmospheric attenuation due to coastal influences, higher humidity, and aerosol concentration typical of Antofagasta's marine boundary layer (Younes, Claywell, and Muneer 2005b). After applying the PER filter, the data distribution becomes denser and more physically consistent, indicating that the correction effectively removed misaligned measurements while preserving the realistic irradiance relationships (Zo et al. 2017).

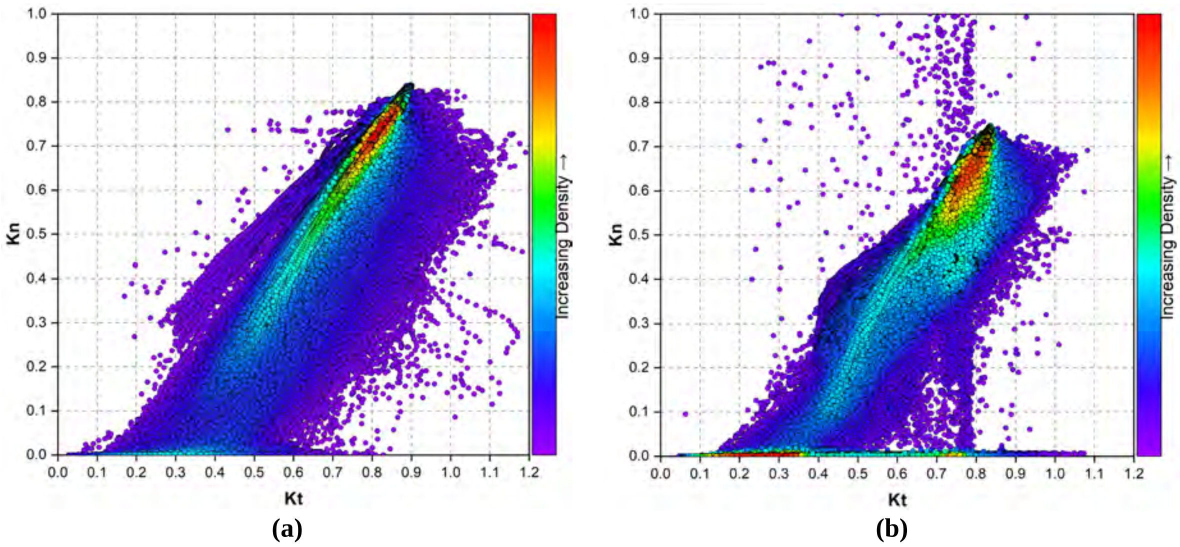

Figure 14: $K_n - K_t$ diagrams for (a) PSDA and (b) CDEA after PER filtering.

5. Conclusions

This work presented a quality analysis of solar radiation data for two locations in northern Chile: PSDA (Atacama Desert) and CDEA (Antofagasta). At both sites, GHI, DNI, and DHI were measured with similar instrumentation at a 1-minute resolution. Eight years of data (April 2017–May 2025) were analyzed for PSDA, and three years (April 2022–May 2025) for CDEA.

A preliminary visual inspection through irradiance heat maps allowed the identification of discontinuities and irregularities. Data losses were estimated at approximately seven and a half months (9%) for PSDA and two weeks (2%) for CDEA. Subsequent filtering and imputation significantly improved data continuity. For PSDA, around 6% of missing GHI and DNI data were recovered using information from nearby instruments, while in CDEA, due to the absence of additional sensors, only data cleaning and filtering were applied.

The application of one-, two-, and three-component analyses (PPL, ERL, and PER) effectively identified and removed anomalous or physically implausible data. The PER limit proved particularly efficient in detecting and filtering DHI and DNI anomalies associated with tracker misalignment and temporary sensor obstruction. Since both components are measured on the same tracker, timestamps of DHI data flagged by PER were also used to filter DNI, ensuring internal consistency.

After all corrections, PSDA retained 92% of valid GHI data, recovered 6%, and left only 2% unavailable. For DHI and DNI, 85.8% of the data passed the filters, 5.3% were detected as anomalous, and 8.9% were unavailable; after recovery, unavailable data decreased to 7.6%. In CDEA, 97% of GHI data were valid, with less than 1% erroneous and 2% unavailable. For DNI and DHI, 81% of the data passed the filters, 17% were classified as erroneous, and 2% were unavailable. The overall data quality and recovery percentages are summarized in Figure 15, which shows the comparative availability and recovery of irradiance components for both stations.

The analysis confirmed that anomalies in GHI were mainly caused by soiling or leveling errors in the pyranometers, while DNI and DHI anomalies were primarily linked to tracker misalignment and dome contamination. The $K_d - K_t$ and $K_n - K_t$ analyses demonstrated that PSDA is dominated by clear-sky conditions ($K_n \approx 0.8$) and minimal atmospheric attenuation, while CDEA shows greater dispersion and lower K_n values (≈ 0.7) due to higher humidity and aerosol concentration typical of its coastal environment.

For CDEA, the behavior patterns observed at PSDA were used as a reference due to the desert's high stability and low cloud variability. Missing data not recovered from ground-based measurements could be complemented with satellite-derived estimates after linear correspondence validation.

The results confirm that systematic quality control substantially improves the reliability of solar irradiance datasets. The combination of visual inspection, multi-component filtering, and PER-based refinement ensures robust detection and correction of anomalies. These procedures also establish a foundation for automated monitoring and alert systems to identify measurement faults in real time, enhancing the accuracy and usability of solar resource assessments in northern Chile.

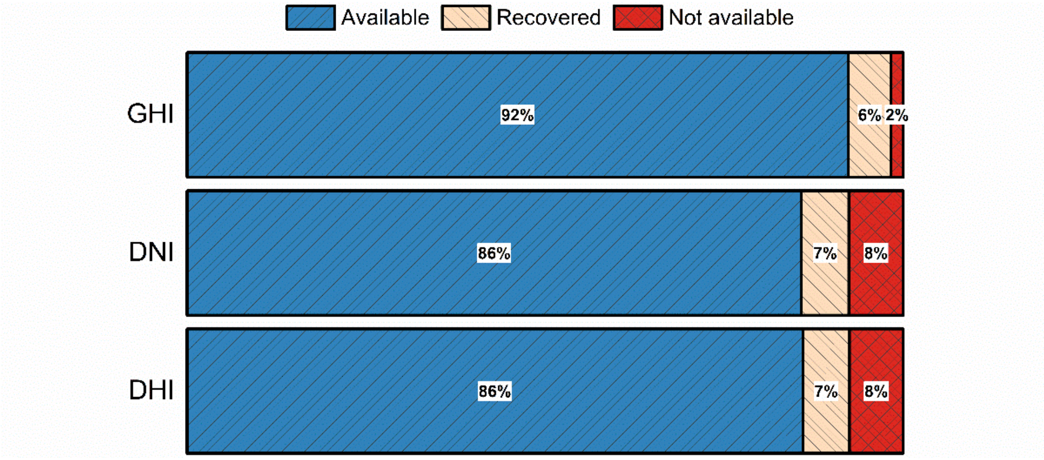

(a)

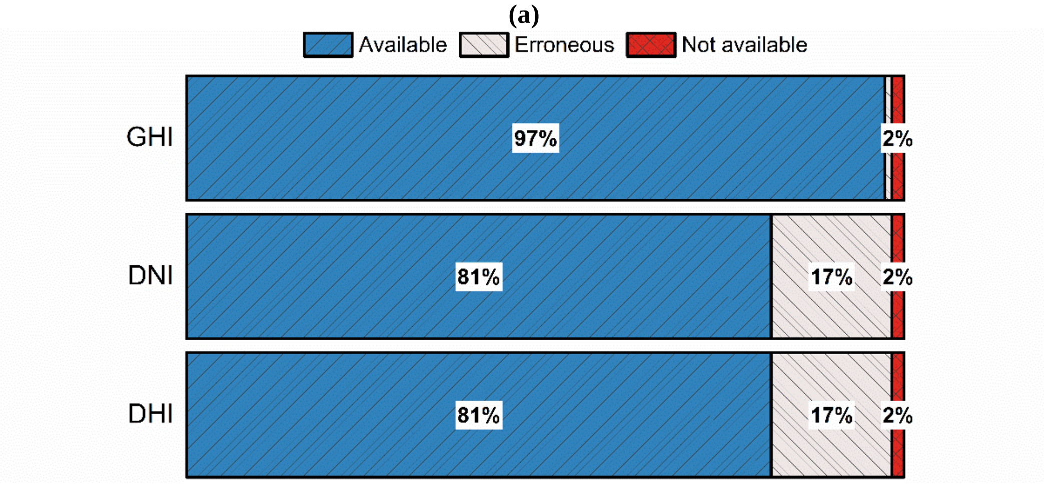

(b)

Figure 15: Summary of data availability, recovery, and loss for (a) PSDA and (b) CDEA after quality control and filtering procedures.

6. Acknowledgements

The authors express gratitude to the projects ANID/FONDAP/1523A0006 "Solar Energy Research Center"-SERC-Chile and the project ATAMOSTEC with the contract no. 17PTECES-75830. The authors also thank the CDEA-UA and the Antofagasta University for the accessibility of the data and the use of their facilities. The authors want to acknowledge the CACTUS project funded by the European Commission in the HORIZON-INFRA-2023-DEV-01-06 program (Ref.: 101132182). Aitor Marzo thanks for the Ramon y Cajal contract (RYC2021-031958-I), funded by the Spanish Ministry of Science and Innovation MCIN/AEI/10.13039/501100011033 and by the European Union "NextGenerationEU/PRTR". This work was partially done by Aitor Marzo during a visit at the University of Antofagasta, supported by the MINEDUC-UA project, code ANT22991.

7. References

El Alani, O, H Ghennioui, A Ghennioui, Y V Saint-Drenan, P Blanc, N Hanrieder, and F-E Dahr. 2021. “A Visual Support of Standard Procedures for Solar Radiation Quality Control.” *International Journal of Renewable Energy Development* 10(3): 401–14. doi:10.14710/ijred.2021.34806.

Anderson, Kevin S., Clifford W. Hansen, William F. Holmgren, Adam R. Jensen, Mark A. Mikofski, and Anton Driesse. 2023. “Pvlib Python: 2023 Project Update.” *Journal of Open Source Software* 8(92): 5994. doi:10.21105/JOSS.05994.

Forstinger, Anne, Stefan Wilbert, Adam R. Jensen, Birk Kraas, Carlos Fernández Peruchena, Chris A. Gueymard, Dario Ronzio, et al. 2021. “Expert Quality Control of Solar Radiation Ground Data Sets.” *Proceedings - ISES Solar World Congress 2021*: 1037–48. doi:10.18086/SWC.2021.38.02.

Gueymard, Christian A., and Jose A. Ruiz-Arias. 2016. “Extensive Worldwide Validation and Climate Sensitivity Analysis of Direct Irradiance Predictions from 1-Min Global Irradiance.” *Solar Energy* 128: 1–30. doi:10.1016/J.SOLENER.2015.10.010.

Kottek, Markus, Jürgen Grieser, Christoph Beck, Bruno Rudolf, and Franz Rubel. 2006. “World Map of the Köppen-Geiger Climate Classification Updated.” *Meteorologische Zeitschrift* 15(3): 259–63. doi:10.1127/0941-2948/2006/0130.

Long, C N, and Y Shi. 2006. “The QCRad Value Added Product: Surface Radiation Measurement Quality Control Testing, Including Climatology Configurable Limits.” *Atmospheric Radiation Measurement Program Technical Report*.

Marzo, A., M. Trigo, J. Alonso-Montesinos, M. Martínez-Durbán, G. López, P. Ferrada, E. Fuentealba, M. Cortés, and F. J. Batlles. 2017. “Daily Global Solar Radiation Estimation in Desert Areas Using Daily Extreme Temperatures and Extraterrestrial Radiation.” *Renewable Energy* 113: 303–11. doi:10.1016/J.RENENE.2017.01.061.

Nollas, Fernando M., German A. Salazar, and Christian A. Gueymard. 2023. “Quality Control Procedure for 1-Minute Pyranometric Measurements of Global and Shadowband-Based Diffuse Solar Irradiance.” *Renewable Energy* 202: 40–55. doi:10.1016/J.RENENE.2022.11.056.

Olivares, D., A. Marzo, A. Taquichiri, R. Espinoza, M. Henriquez, C. Portillo, P. Ferrada, et al. 2025. “Impact of Thermoelectric Coal-Fired Power Plant Emissions on the Soiling Mechanisms of Nearby Photovoltaic Power Plants in the Atacama Desert.” *Renewable Energy* 244: 122684. doi:10.1016/J.RENENE.2025.122684.

Palmer, Diane, Elena Koubli, Ian Cole, Tom Betts, and Ralph Gottschalg. 2018. “Satellite or Ground-Based Measurements for Production of Site Specific Hourly Irradiance Data: Which Is Most Accurate and Where?” *Solar Energy* 165: 240–55. doi:10.1016/J.SOLENER.2018.03.029.

repositorio.smn.gob.ar, Rodrigo Alonso-Suárez, Gonzalo Abal, Raúl Righini, Fernando Martín Nollas, Fernando Ramos-Martins, Olga de Castro Vilela, et al. 2024. “Repositorio Servicio Meteorológico Nacional República Argentina.” http://repositorio.smn.gob.ar/handle/20.500.12160/2741 (September 29, 2024).

Younes, S., R. Claywell, and T. Muneer. 2005a. “Quality Control of Solar Radiation Data: Present Status and Proposed New Approaches.” *Energy* 30(9): 1533–49. doi:10.1016/J.ENERGY.2004.04.031.

Younes, S., R. Claywell, and T. Muneer. 2005b. “Quality Control of Solar Radiation Data: Present Status and Proposed New Approaches.” *Energy* 30(9): 1533–49. doi:10.1016/J.ENERGY.2004.04.031.

Zamalloa-Jara, Marco Antonio, Miguel Ángel Sevillano-Bendezú, Carolin Ulbrich, Gustavo Nofuentes, Rolf Grieseler, and Jan Amaru Töfflinger. 2023. “Overirradiance Conditions and Their Impact on the Spectral Distribution at Low- and Mid-Latitude Sites.” *Solar Energy* 259: 99–106. doi:10.1016/J.SOLENER.2023.05.010.

Zo, Il Sung, Joon Bum Jee, Bu Yo Kim, and Kyu Tae Lee. 2017. “Baseline Surface Radiation Network (BSRN) Quality Control of Solar Radiation Data on the Gangneung-Wonju National University Radiation Station.” *Asia-Pacific Journal of Atmospheric Sciences* 53(1): 11–19. doi:10.1007/S13143-016-0029-5/METRICS.